Thermodynamic stability and properties of boron subnitrides from first principles

A. Ektarawong,[1,*] S. I. Simak,[2] and B. Alling[1,3]

[1]*Thin Film Physics Division, Department of Physics, Chemistry and Biology (IFM), Linköping University, SE-581 83 Linköping, Sweden*

[2]*Theoretical Physics Division, Department of Physics, Chemistry and Biology (IFM), Linköping University, SE-581 83 Linköping, Sweden*

[3]*Max-Planck-Institut für Eisenforschung GmbH, D-40237 Düsseldorf, Germany*

(Received 19 December 2016; published 24 February 2017)

We use the first-principles approach to clarify the thermodynamic stability as a function of pressure and temperature of three different α-rhombohedral-boron-like boron subnitrides, with the compositions of B_6N, $B_{13}N_2$, and $B_{38}N_6$, proposed in the literature. We find that, out of these subnitrides with the structural units of B_{12}(N-N), B_{12}(NBN), and $[B_{12}(N-N)]_{0.33}[B_{12}(NBN)]_{0.67}$, respectively, only $B_{38}N_6$, represented by $[B_{12}(N-N)]_{0.33}[B_{12}(NBN)]_{0.67}$, is thermodynamically stable. Beyond a pressure of about 7.5 GPa depending on the temperature, also $B_{38}N_6$ becomes unstable, and decomposes into cubic boron nitride and α-tetragonal-boron-like boron subnitride $B_{50}N_2$. The thermodynamic stability of boron subnitrides and relevant competing phases is determined by the Gibbs free energy, in which the contributions from the lattice vibrations and the configurational disorder are obtained within the quasiharmonic and the mean-field approximations, respectively. We calculate lattice parameters, elastic constants, phonon and electronic density of states, and demonstrate that $[B_{12}(N-N)]_{0.33}[B_{12}(NBN)]_{0.67}$ is both mechanically and dynamically stable, and is an electrical semiconductor. The simulated x-ray powder-diffraction pattern as well as the calculated lattice parameters of $[B_{12}(N-N)]_{0.33}[B_{12}(NBN)]_{0.67}$ are found to be in good agreement with those of the experimentally synthesized boron subnitrides reported in the literature, verifying that $B_{38}N_6$ is the stable composition of α-rhombohedral-boron-like boron subnitride.

DOI: 10.1103/PhysRevB.95.064206

I. INTRODUCTION

Owing to its unique chemical bonds, boron displays a large number of structures not only as three-dimensional bulk crystals, but also as two-dimensional layers [1–3] and possibly one-dimensional forms [4,5]. As for the three-dimensional bulk crystals, in particular icosahedral boron-rich solids, governed by the three-center two-electron chemical bonds, they exhibit several outstanding properties, such as high chemical stability, high hardness, high melting point, and low wear coefficient [6–13]. Together with the small atomic mass of boron and low density of the compounds, they are thus promising materials for a wide range of technological applications [6,13–21]. For this reason, icosahedral boron-rich solids have become attractive to researchers and have been extensively studied both experimentally and theoretically over the past decades. Among those, icosahedral boron-rich solids with structures related to α-rhombohedral boron (αR-boron), in particular boron carbide, but also boron suboxide, and boron subpnictides, have frequently been addressed in the literature [6–27]. On the contrary, relatively few studies have been made on boron subnitride [28–34], leaving inconclusive issues, regarding its stable compositions, properties, as well as the correct representation of its atomic configuration.

The existence of αR-boron-like boron subnitride was suggested by Condon *et al.* [28], where they examined the gas-solid reaction between boron and nitrogen at elevated temperature, followed by Saitoh *et al.* [29], as they claimed the synthesis of boron nitride thin films with αR-boron-like structure using chemical vapor deposition. However, the information about the composition and the atomic configuration of the as-synthesized boron subnitrides was not provided in either of their studies. Hubert *et al.* [30] synthesized αR-boron-like boron subnitride through solid-state reactions between amorphous boron and hexagonal boron nitride (h-BN) at ∼7.5 GPa and ∼2000 K. By analyzing the data obtained from parallel electron energy-loss spectroscopy and powder x-ray diffraction, they claimed that the as-synthesized subnitride has a composition of $B_6N_{0.92}$ (∼13.29 at. % N) and exhibit a similar crystal structure to that of boron suboxide (B_6O), where B_{12} icosahedra are located at vertices of a rhombohedral unit cell ($R\bar{3}m$ space group) together with a pair of N atoms occupying the interstice between the icosahedra along the [111] direction of the rhombohedron. Based on their conclusion, the structural unit of the ideally stoichiometric B_6O-like boron subnitride, denoted by B_6N (14.28 at. % N), can thus be represented by B_{12}(N-N), where "-" stands for a vacancy residing between the two N atoms, as shown by Fig. 1(a). Solozhenko *et al.* [35] studied *in situ* interaction between β-boron and h-BN under the same pressure-temperature conditions, i.e., at ∼7.5 GPa and ∼2000 K. However, the formation of the B_6O-like boron subnitride was not observed.

Further experimental syntheses of αR-boron-like boron subnitride were later carried out by Solozhenko and Kurakevych [31,32]. In this case, the subnitride was synthesized by crystallization through the peritectic reaction from the mixture between h-BN and liquid boron at 5 GPa. By performing the Rietveld analysis of the diffraction patterns obtained from x-ray powder diffraction, they proposed that the subnitride has a stoichiometric composition of $B_{13}N_2$ (13.33 at. % N), whose crystal structure is similar to that of B_6N but the N-N units are replaced by NBN intericosahedral chains, in an analogy to the idealized picture of $B_{13}C_2$ composition of boron carbide [36–39]. The structural unit of $B_{13}N_2$ is thus given by B_{12}(NBN), as shown in Fig. 1(b). Besides, due to

*anekt@ifm.liu.se

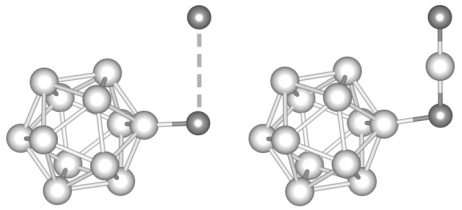

FIG. 1. Structural units of two different αR-boron-like boron subnitrides, proposed in the literature: (a) B_6N or B_{12}(N-N) with 14.28 at. % N, and (b) $B_{13}N_2$ or B_{12}(NBN) with 13.33 at. % N. $B_{38}N_6$ with 13.63 at. % N can be viewed as an alloy of the two in the form of $[B_{12}(N-N)]_{0.33}[B_{12}(NBN)]_{0.67}$. White and grey spheres represent boron and nitrogen atoms, respectively.

the small variation of lattice parameters of the as-synthesized αR-boron-like boron subnitrides in all their experiments, they suggested that αR-boron-like boron subnitride, instead of a solid solution, is an individual line compound [32]. Recently, Zhang *et al.* [34] have proposed an alternative structural model of αR-boron-like boron subnitride, having a composition of $B_{38}N_6$ (13.63 at. % N). The model is represented by a mixture between B_{12}(NBN) and B_{12}(N-N) with a ratio of 2:1, and thus can be written as $[B_{12}(N-N)]_{0.33}[B_{12}(NBN)]_{0.67}$. The importance of the configuration of the two structural units included in the mixture was, however, not discussed. Adding to the complexity, due to the incompleteness of the reactions, the as-synthesized αR-boron-like boron subnitride has often poor crystalline quality and has always been found in a mixture with β-boron, *h*-BN, and α-tetragonal-boron-like boron subnitride, denoted by t-$B_{50}N_{2-x}B_x$ [32,33]. For this reason, exploring the properties of αR-boron-like boron subnitride in experiments is difficult.

In order to answer to the question of which compositions of αR-boron-like boron subnitride that are stable, the thermodynamic stability of the three proposed boron subnitrides, B_{12}(N-N), B_{12}(NBN), and $[B_{12}(N-N)]_{0.33}[B_{12}(NBN)]_{0.67}$, at different pressures and temperatures needs to be determined. The study of high-temperature and high-pressure conditions are motivated as αR-boron-like boron subnitrides are generally synthesized at such conditions.

In this work, we investigate the thermodynamic stability as a function of pressure and temperature of the three αR-boron-like boron subnitrides with respect to their relevant competing phases, using first-principles calculations. The stability of the three subnitrides is determined by the Gibbs free energy, in which the temperature-dependent effects, i.e., the contributions from the lattice vibration and the configurational disorder, are obtained within the quasiharmonic and the mean-field approximations, respectively. We determine the phase diagrams and find that, among the three considered subnitrides, only $[B_{12}(N-N)]_{0.33}[B_{12}(NBN)]_{0.67}$ is thermodynamically stable, and that is so up to a pressure of ~7.5 GPa. Beyond this pressure, $[B_{12}(N-N)]_{0.33}[B_{12}(NBN)]_{0.67}$ becomes unstable, and decomposes into cubic boron nitride (*c*-BN) and t-$B_{50}N_2$, stable within a limited stability range, before it subsequently decomposes upon increasing pressure into pure boron and *c*-BN. We furthermore examine the properties of $[B_{12}(N-N)]_{0.33}[B_{12}(NBN)]_{0.67}$, i.e., elastic constants, phonon and electronic density of states, and demonstrate that $[B_{12}(N-N)]_{0.33}[B_{12}(NBN)]_{0.67}$ is both mechanically and dynamically stable, and is an electrical semiconductor. Our findings are in good agreement in terms of conditions for experimental syntheses of αR-boron-like boron subnitrides, reported in the literature [28–32,40].

TABLE I. Different cell sizes and the corresponding **k**-point grids for Brillouin-zone integration, used in the calculations for the three subnitrides and their relevant competing phases.

Phase	Cell size (number of atoms)	**k**-point grids
αR-boron	$1\times1\times1$ (12)	$9\times9\times9$
	$2\times2\times2$ (96)	$7\times7\times7$
γ-boron	$1\times1\times1$ (28)	$9\times9\times9$
	$2\times2\times2$ (224)	$7\times7\times7$
t-$B_{50}N_2$	$1\times1\times1$ (52)	$9\times9\times9$
	$1\times1\times2$ (104)	$7\times7\times7$
B_{12}(NBN)	$1\times1\times1$ (15)	$9\times9\times9$
	$2\times2\times2$ (120)	$7\times7\times7$
$B_{38}N_6$[a]	$3\times2\times2$ (176)	$3\times5\times5$
B_{12}(N-N)	$1\times1\times1$ (14)	$9\times9\times9$
	$2\times2\times2$ (112)	$7\times7\times7$
c-BN	$1\times1\times1$ (8)	$9\times9\times9$
	$2\times2\times2$ (64)	$7\times7\times7$

[a]$B_{38}N_6$ is represented by $[B_{12}(N-N)]_{0.33}[B_{12}(NBN)]_{0.67}$.

II. METHODOLOGY

A. Computational details

The total energy calculations are performed within the density functional theory (DFT), and the projector augmented wave (PAW) method [41], as implemented in the Vienna *ab initio* simulation package (VASP) [42,43], and the generalized gradient approximation (GGA), proposed by Perdew, Burke, and Ernzerhof (PBE96), for exchange-correlation functional [44]. A plane-wave energy cutoff of 600 eV is used and the Monkhorst-Pack **k**-point mesh [45] is chosen for the Brillouin-zone integration. Since various supercell sizes are used in the calculations, depending on compositions in the binary boron-nitrogen system, we employ different **k**-point grids, listed in Table I, in order to obtain a good accuracy of the total energy within a reasonable computational time. The equilibrium volume at 0 K, denoted by V_0, is determined by the minimum point of the total energy curve $E_0(V)$, calculated for a set of different fixed volumes V. For each volume, the internal atomic positions and the cell shape are fully relaxed so that the total force, acting on each atom, is less than 10^{-6} eV/Å. The tetrahedron method for the Brillouin-zone integrations, suggested by Blöchl [46], is used for electronic density-of-states calculations.

B. Modeling $[B_{12}(N-N)]_{0.33}[B_{12}(NBN)]_{0.67}$

In the present work, a structural model of $B_{38}N_6$, proposed as a stable composition in Ref. [34], is achieved as a disordered $[B_{12}(N-N)]_{0.33}[B_{12}(NBN)]_{0.67}$ alloy using the superatom-special quasirandom structure (SA-SQS) approach for modeling configurational disorder in boron carbide [39,47]

as well as mixing alloys between boron carbide and boron suboxide [48]. The model is constructed within a $3 \times 2 \times 2$ supercell (176 atoms), where two types of superatoms, (1) B_{12}(NBN) and (2) B_{12}(N-N), are randomly distributed on the lattice sites with a ratio of 2 to 1, and thus represented by $[B_{12}(N-N)]_{0.33}[B_{12}(NBN)]_{0.67}$. The Warren-Cowley short-range-order (SRO) parameters between the superatoms for the SA-SQS modeling of $[B_{12}(N-N)]_{0.33}[B_{12}(NBN)]_{0.67}$ are zero for the first two coordination shells.

A detailed investigation of the configuration of the two superatom types in $B_{38}N_6$, beyond the mean-feld approximation, is also performed using the cluster expansion method, and it will be discussed in Sec. III C.

C. Thermodynamic stability

The thermodynamic stability of the boron subnitrides with respect to their competing phases at different pressures p and temperatures T is determined by the Gibbs free energy $G(T,p)$;

$$G(T,p) = E_0(V) + F_{\text{vib}}(T,V) - TS_{\text{conf}}(T,V) + pV. \quad (1)$$

$E_0(V)$ is the total energy at 0 K, directly obtained from the DFT calculations. The contributions from the lattice dynamics (phonons) is given by the Helmholtz free energy $F_{\text{vib}}(T,V)$,

$$F_{\text{vib}}(T,V) = \frac{1}{2}\sum_{\mathbf{q},\nu}\hbar\omega(\mathbf{q},\nu,V) + k_BT\sum_{\mathbf{q},\nu}\ln\{1-\exp[-\hbar\omega(\mathbf{q},\nu,V)/k_BT]\}, \quad (2)$$

where $\omega(\mathbf{q},\nu,V)$ is the phonon frequency at the wave vector $\mathbf{q}$ and the band index ν. $\hbar$ and k_B are the reduced Planck constant and the Boltzmann constant, respectively. In this work, the phonon frequencies ω are also volume dependent, since the phonon calculations are performed within the quasiharmonic approximation, using the PHONOPY package for phonon calculations [49,50]. The force constants for each phase are calculated within supercells, as listed in Table I, using the Parlinski-Li-Kawazoe method [51] with a finite displacement of 0.01 Å. The supercells are then sampled with $21 \times 21 \times 21$ Monkhorst-Pack $\mathbf{k}$-point grids in order to secure the convergence of the phonon frequencies and thus $F_{\text{vib}}(T,V)$.

The term $TS_{\text{conf}}(T,V)$ in Eq. (1) is a contribution from the configurational disorder, where S_{conf} is defined as the configurational entropy. In the present work, S_{conf} is derived within the mean-field approximation, and is volume and temperature independent,

$$S_{\text{conf}} = k_B\ln(g), \quad (3)$$

where g is the number of distinguishable ways of arranging the atoms on the lattice sites. In the case of $[B_{12}(N-N)]_{0.33}[B_{12}(NBN)]_{0.67}$, with the exception of the cluster expansion study in Sec. III C, we assume that the material has maximal configurational disorder between the B_{12}(N-N) and B_{12}(NBN) superatoms, that is a random superatom alloy, with corresponding entropy. The configurational entropy S_{conf}, given in Eq. (3), can thus be approximated within the thermodynamics limit using Stirling's approximation to be

$$S_{\text{conf}} = -k_BN\sum_i x_i\ln(x_i), \quad (4)$$

where N and x_i are defined as the number of lattice sites and the concentration of type i atoms/superatoms.

To determine the term pV and include it in $G(T,p)$ at fixed temperatures, the sums of the first three terms on the right-hand side of Eq. (1) at different fixed volumes are fitted to the third-order Birch-Murnaghan equation of state (EOS) [52,53]. The pressure p is thus calculated by

$$p = -\left[\frac{\partial[E_0(V) + F_{\text{vib}}(T,V) - TS_{\text{conf}}]}{\partial V}\right]_T. \quad (5)$$

D. Elastic properties calculations

In the present work, the elastic properties of the three subnitrides are calculated at $p = 0$ GPa and $T = 0$ K, irrespective of the influence of the zero-point motion. Thus, the Gibbs free energy G, given in Eq. (1), is only determined by the ground-state energy $E_0(V_0)$. To calculate the elastic constants C_{ij}, we apply strains ϵ with $\pm1\%$ and $\pm2\%$ distortions to the supercells with fully relaxed internal atomic positions without volume conservation, and the elastic constants C_{ij} can directly be obtained from the second-order Taylor expansion of the total energy E_0 [54,55],

$$C_{ij} = \frac{1}{V_0}\frac{\partial^2E_0(\epsilon_1,\ldots,\epsilon_6)}{\partial\epsilon_i\partial\epsilon_j}\bigg|_0, \quad (6)$$

where Voigt's notation is used to describe the strain ϵ_i and the elastic tensor C_{ij} [56,57]. $E_0(\epsilon_1,\ldots,\epsilon_6)$, is the total energy of the supercell, distorted by the correspondingly applied strains ϵ_i, whiles V_0 is the equilibrium volume of the undistorted supercell. Since the SQS technique in principle breaks the point-group symmetry of $[B_{12}(N-N)]_{0.33}[B_{12}(NBN)]_{0.67}$, we employ the projection technique, suggested by Moakher *et al.* [58], to derive the rhombohedrally averaged elastic constants $\bar{C}_{ij}$, following the procedure described in Ref. [48] for boron carbide and boron suboxide. Consequently, 12 independent elastic constants in total, i.e., C_{11}, C_{12}, C_{13}, C_{14}, C_{22}, C_{23}, C_{24}, C_{33}, C_{44}, C_{55}, C_{56}, and C_{66}, must be calculated to obtain the six averaged elastic constants, given by

$$\bar{C}_{11} = \tfrac{3}{8}(C_{11}+C_{22}) + \tfrac{1}{4}C_{12} + \tfrac{1}{2}C_{66}, \quad (7a)$$
$$\bar{C}_{12} = \tfrac{1}{8}(C_{11}+C_{22}) + \tfrac{3}{4}C_{12} - \tfrac{1}{2}C_{66}, \quad (7b)$$
$$\bar{C}_{13} = \tfrac{1}{2}(C_{13}+C_{23}), \quad (7c)$$
$$\bar{C}_{14} = \tfrac{1}{4}C_{14} - \tfrac{1}{4}C_{24} + \tfrac{1}{2}C_{56}, \quad (7d)$$
$$\bar{C}_{33} = C_{33}, \quad (7e)$$
$$\bar{C}_{44} = \tfrac{1}{2}C_{44} + C_{55}, \quad (7f)$$
$$\bar{C}_{66} = \tfrac{1}{2}(\bar{C}_{11} - \bar{C}_{12}). \quad (7g)$$

The mechanical stability of the subnitrides is verified by the Born stability criteria [59] for the rhombohedral structure,

$$\bar{C}_{11} - |\bar{C}_{12}| > 0, \quad (8a)$$
$$(\bar{C}_{11} + \bar{C}_{12})\bar{C}_{33} - 2(\bar{C}_{13})^2 > 0, \quad (8b)$$

$$(\bar{C}_{11} - \bar{C}_{12})\bar{C}_{44} - 2(\bar{C}_{14})^2 > 0, \quad (8c)$$

$$\bar{C}_{44} > 0. \quad (8d)$$

The Voigt-Reuss-Hill (VRH) method for determining elastic properties of polycrystalline solids [60] is used to calculate the isotropic elastic Young's, shear, bulk moduli, and Poisson's ratio of boron subnitrides.

III. RESULTS AND DISCUSSION

A. Thermodynamic stability of α-rhombohedral-boron-like boron subnitrides and their relevant competing phases at $T = 0$ K

We first examine the thermodynamic stability at $T = 0$ K of αR-boron-like boron subnitrides. By performing spin-polarized calculations to the three subnitrides, we find that B_{12}(NBN) favors a magnetic state with a magnetic moment of $1\mu_B$, which is in accord with the previous calculations, done by Gou *et al.* [61]. The two other compositions, B_6N and $B_{38}N_6$, resulted in nonmagnetic solutions, even though the calculations were started with nonzero magnetic moments. As a result, further investigation of B_{12}(NBN) will be carried out within the spin-polarized DFT framework, while the other compositions are treated as non-spin-polarized. We neglect the influence of lattice dynamics at $T = 0$ K, i.e., the zero-point motion, so the Gibbs free energy G, given in Eq. (1), reduces to the enthalpy H;

$$H(p) = E_0(V) + pV. \quad (9)$$

Consequently, the stability of the three subnitrides at different fixed pressures can be determined by calculating the formation enthalpy ΔH^{form} with respect to their relevant competing phases, i.e., pure boron and boron nitride, as shown in Fig. 2. As for pure boron, we consider αR-boron as a competing phase of the subnitrides at low pressure. Upon increasing pressure, αR-boron undergoes a phase transition into γ-boron, which should also be included when determining the stability of the subnitrides under high pressure. According to our calculations at $T = 0$ K, the transition from αR- to γ-boron is predicted to take place at $p = 18.8$ GPa, which is in good agreement with the values reported in the literature [62,63]. In the case of boron nitride, due to the fact that standard DFT calculations cannot accurately describe the van der Waals interactions between the boron nitride layers of the hexagonal phase (h-BN), only the cubic phase (c-BN) is considered as a competing phase for the subnitride. However, as demonstrated by a number of experimental and theoretical works [64–69], it is generally accepted that c-BN is thermodynamically stable over h-BN at zero pressure and zero temperature conditions, and is also found to be stable up to relatively high pressures and high temperatures.

Since the formation of α-tetragonal-boron-like phase, given by t-$B_{50}N_{2-x}B_x$, has also been reported in the experimental syntheses of αR-boron-like boron subnitride [32,33], we consider the stoichiometric t-$B_{50}N_2$ as one of the competing phases for the three αR-boron-like boron subnitrides. We note that the representation of the atomic configuration of t-$B_{50}N_2$ has still not been decisive due to a variety of ways for individual boron and nitrogen atoms to fully and/or partially occupy

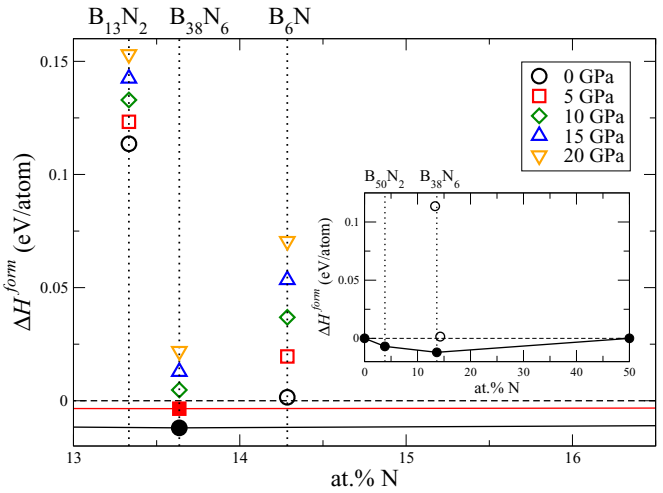

FIG. 2. Formation enthalpy ΔH^{form} of t-$B_{50}N_2$, B_{12}(NBN), $[B_{12}(N-N)]_{0.33}[B_{12}(NBN)]_{0.67}$, and B_{12}(N-N), corresponding to the compositions of $B_{50}N_2$, $B_{13}N_2$, $B_{38}N_6$, and B_6N respectively, with respect to pure boron (αR and γ phases) and c-BN under pressures, ranging from 0 to 20 GPa. Filled and open symbols indicate compositions, which are lying on and above the convex hulls at different fixed pressures, respectively. The inset shows a full picture of the convex hull at $p = 0$ GPa.

different interstitial sites [70–72]. In the present work, the atomic configuration of t-$B_{50}N_2$, recently proposed by Uemura *et al.* [72] is chosen, as it is found to be the lowest-energy configuration, among several considered possible occupations of the interstitial atoms. The configuration is represented by (1) four icosahedral clusters, centered at ($a/4$, $a/4$, $c/4$), ($3a/4$, $3a/4$, $c/4$), ($3a/4$, $a/4$, $3c/4$), and ($a/4$, $3a/4$, $3c/4$) of the tetragonal unit cell, (2) two interstitial boron atoms, partially placed either at the 8h or at the 8i sites, and (3) two interstitial nitrogen atoms, located at the 2b sites.

As can be seen from the inset in Fig. 2, only $B_{38}N_6$, as represented by $[B_{12}(N-N)]_{0.33}[B_{12}(NBN)]_{0.67}$, and t-$B_{50}N_2$ are lying on the convex hull at zero pressure. The other compositions, B_6N and $B_{13}N_2$, on the other hand, are found to be above the hull by 13 and 125 meV/atom, respectively. We also find that ΔH^{form} of the three boron subnitrides as well as t-$B_{50}N_2$ increases with the pressure, and $[B_{12}(N-N)]_{0.33}[B_{12}(NBN)]_{0.67}$ becomes unstable with respect to t-$B_{50}N_2$ and c-BN at $p \approx 6$ GPa. t-$B_{50}N_2$ subsequently decomposes into αR-boron and c-BN at $p > 7$ GPa.

B. Structural, electronic, and elastic properties of α-rhombohedral-boron-like boron subnitrides

As a next step, we investigate the ground-state properties of the three αR-boron-like boron subnitrides. Table II shows the lattice parameters a, angles α, and the unit-cell volumes of the three subnitrides, calculated in the present work. We note that the lattice parameters (a, b, c), and also the angles between them (α, β, γ) of boron subnitride at $B_{38}N_6$ composition, represented by $[B_{12}(N-N)]_{0.33}[B_{12}(NBN)]_{0.67}$, are slightly deviating from each other by less than 1%. This is attributed to the use of SA-SQS technique, breaking the point-group symmetry due to its finite size of the SQS supercell, for modeling

TABLE II. Lattice parameters a, angles α, and unit-cell volumes V_0 of α-rhombohedral-boron-like boron subnitrides, calculated in the present work. Comparison is made with experiments and previous calculations.

Composition	a (Å/unit cell)	α (°)	V_0 (Å^3/unit cell)
Experiments			
$B_6N_{0.92}$	5.155[a]	63.91[a]	105.228[a]
$B_{13}N_2$	5.159[b]	63.88[b]	105.389[b]
	5.157[c]	63.73[c]	104.990[c]
Calculations			
B_6N	5.146	63.83	104.543
$B_{13}N_2$	5.219	63.44	108.206
	5.209[d]	63.45[d]	107.591[d]
$B_{38}N_6$[e]	5.158	63.78	105.129

[a]Reference [30]: Hubert *et al.* (x-ray diffraction).
[b]Reference [31]: Solozhenko *et al.* (x-ray diffraction).
[c]Reference [32]: Solozhenko *et al.* (x-ray diffraction).
[d]Reference [61]: Gou *et al.* (spin-polarized GGA-PBE96).
[e]$B_{38}N_6$ is represented by $[B_{12}(N-N)]_{0.33}[B_{12}(NBN)]_{0.67}$.

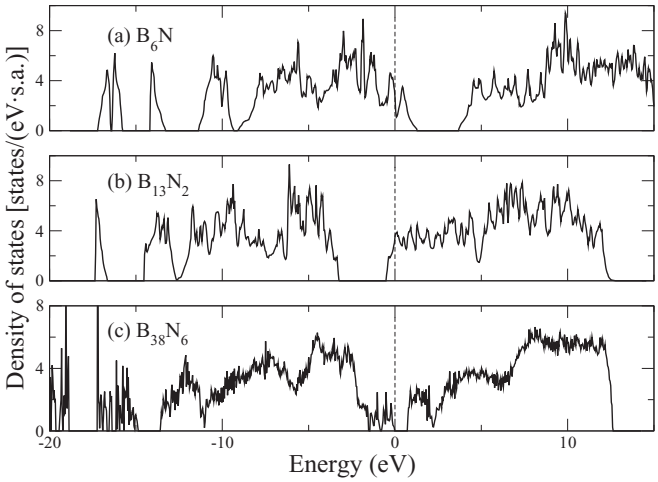

FIG. 3. Electronic density of states of (a) B_6N, (b) $B_{13}N_2$, and (c) $B_{38}N_6$, represented by B_{12}(N-N), (b) B_{12}(NBN), and (c) $[B_{12}(N-N)]_{0.33}[B_{12}(NBN)]_{0.67}$, respectively. The dashed lines at 0 eV indicate the highest energy states, occupied by the electrons.

$[B_{12}(N-N)]_{0.33}[B_{12}(NBN)]_{0.67}$. For this reason, the lattice parameters and the angles of $[B_{12}(N-N)]_{0.33}[B_{12}(NBN)]_{0.67}$, given in Table II, are rhombohedrally averaged. As can be seen from Table II, the calculated lattice parameters of all three compositions considered are in general agreement with the experimental values. However, judging from our previous works on related icosahedral boron-rich systems [47], we expect that our PAW-GGA calculations should be extremely close to the measured values, when the correct atomic configurations are used. Thus, we can see that in particular the calculated lattice parameters and volume at $B_{13}N_2$ composition, given by B_{12}(NBN), substantially deviate from experiments. For example, the calculated volume of B_{12}(NBN) is larger than those measured from the experiments by more than 2%. In addition, we find that the calculated lattice parameters and volume of $[B_{12}(N-N)]_{0.33}[B_{12}(NBN)]_{0.67}$ at $B_{38}N_6$ composition, whose volume differs from the experiments by less than 0.25%, are found to be in even better agreement with the experiments than those of B_{12}(N-N) at B_6N composition. The match of lattice parameters and volume between those calculated for $[B_{12}(N-N)]_{0.33}[B_{12}(NBN)]_{0.67}$ and the experiments strengthens our findings in the previous section that $B_{38}N_6$ is the stable composition for αR-boron-like boron subnitride.

By considering the electronic density of states of the three αR-boron-like boron subnitrides, as shown in Fig. 3, we find that $[B_{12}(N-N)]_{0.33}[B_{12}(NBN)]_{0.67}$ is an electrical semiconductor with a GGA-based electronic band gap of 0.7 eV, while B_{12}(N-N) and B_{12}(NBN) are both metallic. The appearance of such electronic characters, observed in the three subnitrides, can be explained by the electron counting rules, proposed by Longuet-Higgins and Roberts [74], for interpreting the electronic structure and stability of icosahedral boron-rich clusters, which has recently been discussed by Zhang *et al.* [34] also for boron subnitrides. The metallic character of B_{12}(N-N) is due to the electron deficiency of the B_{12} icosahedron, in which two more electrons are required to complete its bonding states. In this case, the Fermi level is located in the valence band. On the one hand, the addition of one extra boron atom to form the B_{12}(NBN) at $B_{13}N_2$ composition gives rise to an excess electron filling an antibonding state of the icosahedron, and thus resulting in the metallic character, where the Fermi level is lying in the conduction band. As a consequence, the $B_{38}N_6$ composition, composed of B_{12}(N-N) and B_{12}(NBN) with a ratio of 1:2, corresponds to the precise electron count, making the system electrically semiconducting.

Table III shows the elastic constants and elastic moduli of the three αR-boron-like boron subnitrides, calculated at $p = 0$ GPa and $T = 0$ K, using the projection technique described in Sec. II D. As can be seen from Table III, the elastic constants as well as bulk and shear moduli of B_{12}(NBN), calculated in this work, are in excellent agreement with the previous calculations, reported by Gou *et al.* [61], thus confirming the reliability of our calculations. By inspecting the mechanical stability of the three subnitrides with the Born stability criteria for the rhombohedral structure, provided by Eq. (8), we verify that all the criteria are fulfilled for the three compositions of boron subnitride, demonstrating that they are all mechanically stable. Recent theoretical works on B_{12}(N-N) [73] and B_{12}N(NBN) [61] have demonstrated elastic constants in line with potentially superhard materials. We thus expect $[B_{12}(N-N)]_{0.33}[B_{12}(NBN)]_{0.67}$, whose calculated elastic moduli are comparable to those calculated for the other two subnitrides, is potentially a superhard material. Beside, the values of the B/G ratio of the three considered subnitrides, given in Table III, are smaller than 1.75, implying that the materials are brittle according to Pugh's criterion [75].

C. Configurational disorder in $[B_{12}(N-N)]_{0.33}[B_{12}(NBN)]_{0.67}$

In this subsection, we examine the influence of configurational disorder, induced either by atomic B/N substitutional defects or by the configuration of the B_{12}(N-N) and B_{12}(NBN) superatoms, on the stability of $[B_{12}(N-N)]_{0.33}[B_{12}(NBN)]_{0.67}$.

TABLE III. Averaged elastic constants $\bar{C}_{ij}$ (GPa), bulk modulus B_H (GPa), shear modulus G_H (GPa), Young's modulus E_H (GPa), Poisson's ratio ν_H, and B_H/G_H ratio in the Voigt-Reuss-Hill (VRH) approach for B_{12}(N-N), B_{12}(NBN), and $[B_{12}(N-N)]_{0.33}[B_{12}(NBN)]_{0.67}$. Comparison is made with previous calculations of B_{12}(N-N) and B_{12}N(NBN).

	$\bar{C}_{11}$	$\bar{C}_{12}$	$\bar{C}_{13}$	$\bar{C}_{14}$	$\bar{C}_{33}$	$\bar{C}_{44}$	B_H	G_H	E_H	ν_H	B_H/G_H	Ref.
B_{12}(N-N) (Calc.)	601	134	50	–8	411	143	225	190	444	0.17	1.19	this work
							236					[73][a]
B_{12}(NBN) (Calc.)	522	135	84	48	538	117	243	157	387	0.23	1.55	this work
	531	130	80		541	108	242	162			1.49	[61][b]
$B_{38}N_6$[c] (Calc.)	511	171	65	63	507	162	236	167	403	0.21	1.41	this work

[a]Reference [73]: Guo *et al.* (ultrasoft pseudo-potential GGA-PBE96).
[b]Reference [61]: Gou *et al.* (spin polarized GGA-PBE96).
[c]$B_{38}N_6$ is represented by $[B_{12}(N-N)]_{0.33}[B_{12}(NBN)]_{0.67}$.

It has recently been demonstrated that configurational disorder plays an important role for the stability as well as the properties of boron carbides at elevated temperature [39,47,48,76]. We first consider different kinds of B/N substitutional defects in the dilute limit, involved with only two atoms, in a fully relaxed $3 \times 2 \times 2$ supercell of $[B_{12}(N-N)]_{0.33}[B_{12}(NBN)]_{0.67}$, as the defect-free structure. In the present work, the substitutional defects are only generated by swapping B and N atoms in the supercell, and thus the global compositions of all defective structures are fixed at $B_{38}N_6$. The defect formation energy, ΔE_{defect}, is calculated by

$$\Delta E_{\text{defect}} = E_{\text{defect}} - E_{\text{defect-free}}, \tag{10}$$

where E_{defect} and $E_{\text{defect-free}}$ are defined as the total energy of the defective and the defect-free structures, respectively. We note that, during the calculations of the defective structures, only the atomic coordinates are relaxed, while their supercell volumes are kept fixed at the equilibrium volume V_0 of the defect-free structure. Some selected low-energy B/N substitutional defects, their formation energy, ΔE_{defect}, and the formation enthalpies, ΔH^{form}, of the defect-free as well as defective structures at zero pressure with respect to c-BN and αR-boron are listed in Table IV.

We find that the formation of the B/N substitutional defects in $[B_{12}(N-N)]_{0.33}[B_{12}(NBN)]_{0.67}$ even in the dilute limit results in an unstable structure, as indicated by the positive formation enthalpies ΔH^{form} with respect to the competing phases. We attribute this to the relatively high energy ΔE_{defect}, at least 4 eV, it costs for a single swap of boron and nitrogen atoms in $[B_{12}(N-N)]_{0.33}[B_{12}(NBN)]_{0.67}$. We thus conclude that configurational disorder, induced by B/N substitutional defects, is unlikely for $[B_{12}(N-N)]_{0.33}[B_{12}(NBN)]_{0.67}$. In order to investigate the influence of configurational disorder in $[B_{12}(N-N)]_{0.33}[B_{12}(NBN)]_{0.67}$ on the B_{12}(N-N) and B_{12}(NBN) superatom level, we calculate so-called effective cluster interactions by solving a set of linear equations, known as the Connolly-Williams cluster expansion (CE) method [77], within the "superatom" framework,

$$E_0^{\gamma} = E_0^{'} + \sum_f V_f^{(n)} \xi_f^{(n)-\gamma}. \tag{11}$$

E_0^{γ} is the total energy of $[B_{12}(N-N)]_{0.33}[B_{12}(NBN)]_{0.67}$ with a given configuration γ. $\xi_f^{(n)-\gamma}$ and $V_f^{(n)}$ are the n-site correlation functions of a specific cluster f, defined for configuration γ, and the n-site effective cluster interactions for a specific cluster f, respectively. $E_0^{'}$ is the total energy of $[B_{12}(N-N)]_{0.33}[B_{12}(NBN)]_{0.67}$, imitating the configuration of random alloy stable in the limit $V/T \rightarrow 0$, where $\xi_f^{(n)} = 0$.

In the present work, $\xi_f^{(n)-\gamma}$ are defined by the Warren-Cowley short-range-order (SRO) parameters, α_i, representing the two-site correlation functions for the ith coordination shell, and thus $V_f^{(n)}$ reduces to $V_i^{(2)}$, which is the effective pair interaction for the ith coordination shell. As a preliminary investigation, we aim at solving for $V_i^{(n)}$ up to the third shell. Equation (11) can thus be rewritten as

$$E_0^{\gamma} = E_0^{'} + \sum_{i=1}^{3} n_i V_i^{(2)} \alpha_i^{\gamma}, \tag{12}$$

where n_i is the number of superatoms in the ith shell. To solve for the unknown quantities in Eq. (12), i.e., $E_0^{'}$ and $V_i^{(2)}$, we model a set of $[B_{12}(N-N)]_{0.33}[B_{12}(NBN)]_{0.67}$ structures, where α_i^{γ} are uniquely defined for each configuration γ, and then determine E_0^{γ}, using DFT calculations. $E_0^{'}$ and $V_i^{(2)}$ can thus be obtained by performing a least-squares fit to the set

TABLE IV. Some of the dilute substitutional defects in $3 \times 2 \times 2$ supercells, and their formation energies, ΔE_{defect}, in eV/defect with respect to $[B_{12}(N-N)]_{0.33}[B_{12}(NBN)]_{0.67}$, as the defect-free structure. Superscript p and e denote *polar* and *equatorial* sites in the icosahedron, respectively, and "-" stands for a vacancy. ΔH^{form} is defined as the formation enthalpy in meV/atom of the defect-free and defective structures at zero pressure with respect to c-BN and αR-boron.

Defective structure	ΔE_{defect} (eV/defect)	ΔH^{form} (meV/atom)
Defect-free structure	0	−12
$B_{11}N^p$(BBN)	4.40	13
$B_{11}N^e$(BBN)	4.22	12
$B_{11}N^e$(NBB)[a]	8.31	35
B_{12}(BNN)	5.45	19
$B_{11}N^p$(B-N)	6.71	26
$B_{11}N^e$(B-N)	4.05	11
$B_{11}N^e$(N-B)[a]	7.46	30
B_{12}(B-N) + B_{12}(NNN)	7.85	32

[a]There exists a N-N bond between the NBB or N-B unit and the $B_{11}N^e$ icosahedron in that defective structure.

of Eq. (12). Table V lists the SRO parameters (α_i; $i = 1$–3) for four configurations of $[B_{12}(N-N)]_{0.33}[B_{12}(NBN)]_{0.67}$, labeled by configuration $\gamma = 1$–4, and their total energies per superatom (s.a.), $E_0^{\gamma-\mathrm{DFT}}$, obtained from DFT calculations. Together with the input from the four structures, we perform the least-square fit to the four corresponding Eq. (12), and obtain the fitting parameters, i.e., $E_0^{'}$, $V_1^{(2)}$, $V_2^{(2)}$, and $V_3^{(2)}$ in eV/s.a., which are given as follows:

$$\begin{pmatrix} E_0^{'} \\ V_1^{(2)} \\ V_2^{(2)} \\ V_3^{(2)} \end{pmatrix} = \begin{pmatrix} -106.268 \\ 0.0011 \\ -0.0071 \\ 0.0031 \end{pmatrix}. \tag{13}$$

The small positive values of $V_1^{(2)}$ and $V_3^{(2)}$ indicate ordering tendencies between superatoms, B_{12}(N-N) and B_{12}(NBN), for the first and third shells, respectively, while the negative value of $V_2^{(2)}$ indicates a tendency to form B_{12}(N-N)-B_{12}(N-N) and B_{12}(NBN)-B_{12}(NBN) pairs at the second shell.

The obtained effective pair interactions $V_i^{(2)}$, given in Eq. (13), are then used in Monte Carlo (MC) simulations in order to search for a possible low-energy configuration of $[B_{12}(N-N)]_{0.33}[B_{12}(NBN)]_{0.67}$, denoted by *ordered* structure, supposedly stable at low temperature. In this case, simulation boxes of $30 \times 30 \times 30$ rhombohedral unit cells (396 000 atoms) are used, and the MC simulations are performed, using the Metropolis *et al.* [78] algorithm, in the temperature range of 0–4000 K, in which the temperature steps are 100 and 50 K for $T > 1400$ K and $T < 1400$ K, respectively. At each temperature, the simulations include 10 000 Monte Carlo steps (MCSs) for equilibrating the system and then 10 000 more MCSs for obtaining the proper averages of the total energies, specific heat, and SRO parameters. The simulations reveal two order-disorder transitions at ~750 and ~1300 K, as indicated by the peaks in the calculated configurational specific heat, c_V, illustrated in Fig. 4. The SRO parameters as well as the total energy $E_0^{\gamma-\mathrm{CE}}$ at $T = 0$ K of $[B_{12}(N-N)]_{0.33}[B_{12}(NBN)]_{0.67}$, representing the ordered structure, are also given in Table V.

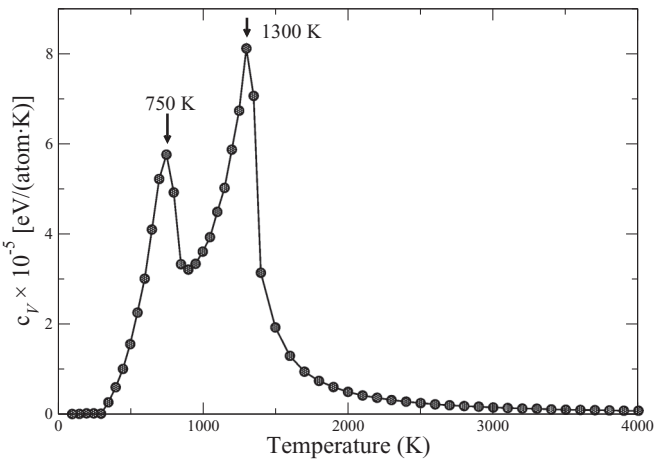

FIG. 4. Specific heat (c_V) of $[B_{12}(N-N)]_{0.33}[B_{12}(NBN)]_{0.67}$, evaluated from Monte Carlo simulations, using simulation boxes of $30 \times 30 \times 30$ rhombohedral unit cells.

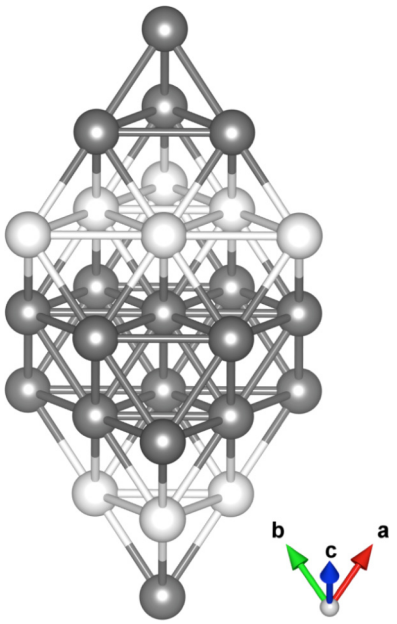

FIG. 5. Superatomic configuration, representing the ordered structure of $[B_{12}(N-N)]_{0.33}[B_{12}(NBN)]_{0.67}$, in which white and grey spheres stand for B_{12}(N-N) superatoms and B_{12}(NBN) superatoms, respectively.

The ordered structure of $[B_{12}(N-N)]_{0.33}[B_{12}(NBN)]_{0.67}$, predicted to be stable at $T < 750$ K, can be viewed from the superatomic perspective as a stacking sequence of two layers of B_{12}(NBN) superatoms and one layer of B_{12}(N-N) superatoms, as depicted in Fig. 5. According to our prediction, the ordered $[B_{12}(N-N)]_{0.33}[B_{12}(NBN)]_{0.67}$ undergoes an order-disorder transition at $T \sim 750$ K to the *intermediate* phase, stable up to $T \sim 1300$ K, where a small amount of B_{12}(N-N) superatoms from the B_{12}(N-N) layers substitutes for B_{12}(NBN) superatoms, residing in the layers of B_{12}(NBN) superatoms, and vice versa, resulting in a stacking sequence of B_{12}(NBN)-rich layers and B_{12}(N-N)-rich layers. At $T \gtrsim 1300$ K, $[B_{12}(N-N)]_{0.33}[B_{12}(NBN)]_{0.67}$ loses configurational long-range order due to thermally activated random arrangement of B_{12}(N-N) and B_{12}(NBN) superatoms.

For comparison, we estimate the order-disorder transition temperature of $[B_{12}(N-N)]_{0.33}[B_{12}(NBN)]_{0.67}$, using the mean-field approximation. In this case, the transition temperature is calculated from the difference in the Gibbs free energy $\Delta G(T)$ between the ordered and disordered structures. Neglecting the influence of zero-point motion, the Gibbs free energy in this case of the ordered and disordered structures is given by

$$G^{\mathrm{ord}}(T) = E_0^{\mathrm{ord}}, \tag{14}$$

and

$$G^{\mathrm{dis}}(T) = E_0^{\mathrm{dis}} - T S_{\mathrm{conf}}, \tag{15}$$

respectively. By assuming that the ordered structure has the zero-temperature properties ($T = 0$ K), while the disordered structure has the $T \to \infty$ properties, E_0^{ord} and E_0^{dis} are given by $E_0^{\gamma-\mathrm{CE}}$ for the ordered structure, listed in Table V, and the fitting parameter $E_0^{'}$, respectively. The

TABLE V. Five configurations of $[B_{12}(N-N)]_{0.33}[B_{12}(NBN)]_{0.67}$, and their Warren-Cowley short-range-order (SRO) parameters (α_i; $i = 1$–3) for the first three coordination shells. $E_0^{\gamma-\mathrm{DFT}}$ and $E_0^{\gamma-\mathrm{CE}}$ stand for the total energies per superatom (s.a.), calculated from DFT and from Eq. (12), together with the fitting parameters, i.e., $E_0^{'}$, $V_i^{(2)}$, obtained from the Connolly-Williams cluster expansion (CE) method [77], respectively.

Configuration γ	Supercell size (no. of atoms)	α_1	α_2	α_3	$E_0^{\gamma-\mathrm{DFT}}$ (eV/s.a.)	$E_0^{\gamma-\mathrm{CE}}$ (eV/s.a.)
1	$3 \times 2 \times 2$ (176)	0	0	–0.125	–106.2703	–106.2703
2	$3 \times 2 \times 2$ (176)	–0.5	0.5	–0.5	–106.3020	–106.3019
3	$3 \times 2 \times 2$ (176)	0.5	0	–0.5	–106.2739	–106.2740
4	$3 \times 3 \times 3$ (396)	0	0	0	–106.2680	–106.2680
Ordered structure	$30 \times 30 \times 30$ (396 000)	–0.5	1.0	–0.5		–106.3232

configurational entropy S_{conf} per s.a. for the *disordered* structure of $[B_{12}(N-N)]_{0.33}[B_{12}(NBN)]_{0.67}$ is then estimated, using Eq. (4), to be

$$S_{\mathrm{conf}} = -k_B\left[\tfrac{1}{3}\ln\left(\tfrac{1}{3}\right) + \tfrac{2}{3}\ln\left(\tfrac{2}{3}\right)\right]. \quad (16)$$

A mean-field estimate of the ordered-disordered transition temperature for $[B_{12}(N-N)]_{0.33}[B_{12}(NBN)]_{0.67}$ is 1061 K, falling between the two order-disorder transition temperatures, predicted by the MC simulations.

D. Lattice dynamics and thermodynamic stability at $T > 0$ K

We also investigate the influence of lattice vibrations on the thermodynamic stability of the three αR-boron-like boron subnitrides. In this work, the vibrational contributions to the Gibbs free energy $G(T,p)$, as denoted by $F_{\mathrm{vib}}(T,V)$, for the three subnitrides and their relevant competing phases, those are αR- and γ-boron, t-$B_{50}N_2$, and c-BN, are calculated within the quasiharmonic approximation, using the approaches described in Sec. II C. We first inspect the phonon density of states of B_{12}(N-N), B_{12}(NBN), and $[B_{12}(N-N)]_{0.33}[B_{12}(NBN)]_{0.67}$, as illustrated in Fig. 6. As can be seen from Fig. 6, the phonon frequencies of B_{12}(N-N) and $[B_{12}(N-N)]_{0.33}[B_{12}(NBN)]_{0.67}$ are all positive, assuring their dynamical stabilities. The phonon density of states of B_{12}(NBN), on the other hand, displays a band of imaginary phonon frequencies, indicating that B_{12}(NBN) is dynamically unstable. Considering that B_{12}(NBN) is dynamically unstable, together with its relatively high formation enthalpy ΔH^{form} with respect to the competing phases (see Fig. 2), we conclude that the stoichiometric $B_{13}N_2$, represented solely by B_{12}(NBN), is not a stable composition of αR-boron-like boron subnitride.

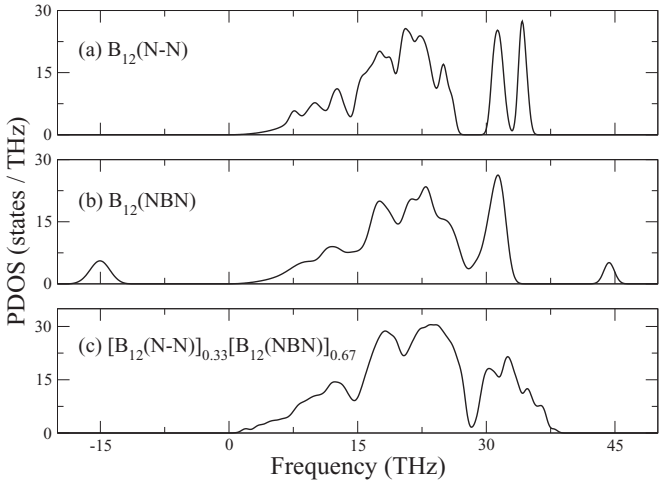

FIG. 6. Phonon density of states (PDOS) of (a) B_{12}(N-N), (b) B_{12}(NBN), and (c) $[B_{12}(N-N)]_{0.33}[B_{12}(NBN)]_{0.67}$, corresponding to the compositions of B_6N, $B_{13}N_2$, and $B_{38}N_6$, respectively, at $p = 0$ GPa. Negative numbers correspond to imaginary frequencies.

We then determine the thermodynamic stability as a function of pressure p and temperature T of B_{12}(N-N) and $[B_{12}(N-N)]_{0.33}[B_{12}(NBN)]_{0.67}$ with respect to the competing phases by calculating the Gibbs free energy $G(T,p)$, given by Eq. (1). It is worth noting that, due to the partial occupation of the two interstitial boron atoms, t-$B_{50}N_2$ has a nonzero configurational entropy S_{conf}. In our case, one-eighth of 8h and of 8i interstitial sites are occupied by the first and second boron atoms, respectively. We thus estimate the configurational entropy S_{conf}/unit cell for t-$B_{50}N_2$, using Eq. (3), to be $k_B\ln(64)$ or $\sim 0.079 k_B$/atom. The configurational entropy S_{conf} for $[B_{12}(N-N)]_{0.33}[B_{12}(NBN)]_{0.67}$ is given by Eq. (16), i.e., $\sim 0.043 k_B$/atom, while it is zero for αR- and γ-boron, c-BN, and B_{12}(N-N).

We find that, in the temperature range from 0 to 2300 K, $[B_{12}(N-N)]_{0.33}[B_{12}(NBN)]_{0.67}$ is thermodynamically stable with respect to all relevant competing phases, including B_{12}(N-N), up to $\sim$7.5 GPa. Beyond this pressure, $B_{38}N_6$, $[B_{12}(N-N)]_{0.33}[B_{12}(NBN)]_{0.67}$ becomes unstable and decomposes into c-BN and t-$B_{50}N_2$, stable within a limited stability range before it subsequently decomposes upon increasing pressure into αR- or γ-boron, depending on the pressure and temperature, and c-BN. The stability range of $[B_{12}(N-N)]_{0.33}[B_{12}(NBN)]_{0.67}$ is displayed through the p-T phase diagram at the composition of $B_{38}N_6$, as illustrated in Fig. 7. As for the stoichiometric B_6N, represented by B_{12}(N-N), we find that it is never stable with respect to $[B_{12}(N-N)]_{0.33}[B_{12}(NBN)]_{0.67}$ and c-BN at any pressure or temperature.

We find that our obtained p-T phase diagram at the global composition of $B_{38}N_6$, shown in Fig. 7, provides a good agreement in terms of conditions for experimental syntheses of αR-boron-like boron subnitrides, reported in the literature [28–32,40]. For example, the experimental syntheses of αR-boron-like boron subnitride, carried out by Hubert

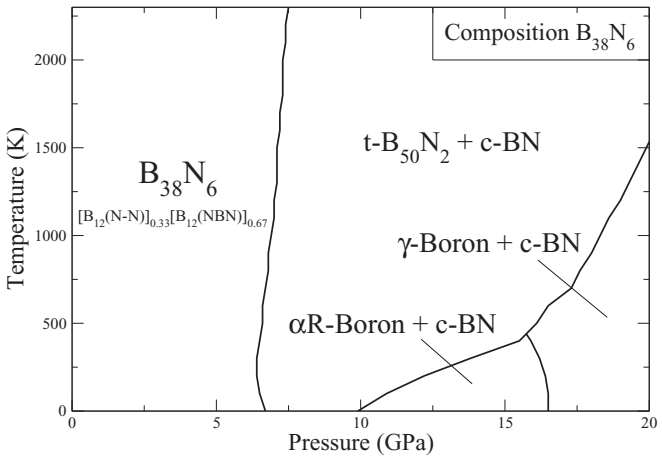

FIG. 7. p-T phase diagram at a composition of $B_{38}N_6$.

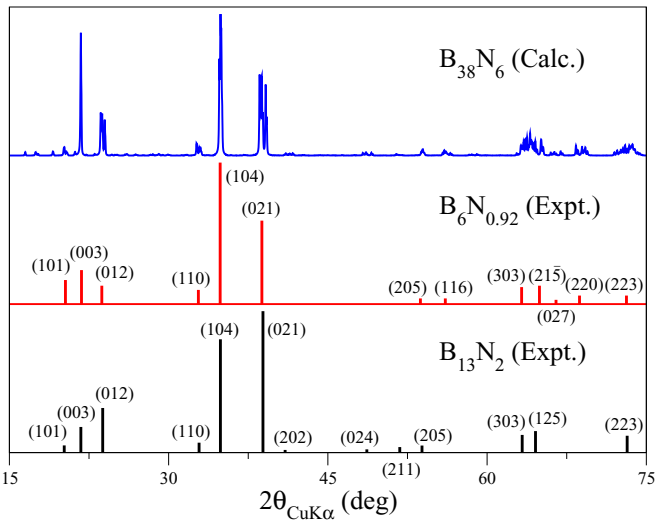

FIG. 8. Simulated x-ray powder-diffraction pattern (Cu$K\alpha$) of $[B_{12}(N-N)]_{0.33}[B_{12}(NBN)]_{0.67}$ at the composition of $B_{38}N_6$ (blue), compared with the experimental powder-diffraction data of $B_6N_{0.92}$ [30] (red) and $B_{13}N_2$ (black), taken from The International Centre for Diffraction Data (ICDD) cards: 00-050-1504 and 00-060-0209, respectively.

et al. [30] through solid-state reactions between boron and h-BN at $p \approx 7.5$ GPa and $T \approx 2000$ K, and Solozhenko and Kurakevych [31,32] upon cooling of the mixture between liquid boron and h-BN from $T > 2300$ K at $p \approx 5$ GPa. We can see that the conditions, used for the syntheses of the subnitrides in both cases, fall into the predicted stability range of $[B_{12}(N-N)]_{0.33}[B_{12}(NBN)]_{0.67}$. As can be seen from Fig. 7, the synthesis of boron subnitride at $p \approx 7.5$ GPa, made by Hubert *et al.* [30], is very close to the boundary where $[B_{12}(N-N)]_{0.33}[B_{12}(NBN)]_{0.67}$ becomes unstable and decomposes into the competing phases. We suggest that this might explain why the formation of αR-boron-like boron subnitride was not observed in the *in situ* experiments, conducted by Solozhenko *et al.* [35], under the same p-T conditions. In addition, Cao *et al.* [40] reported the experimental synthesis of αR-boron-like boron subnitride at low pressure ($\sim 10^{-5}$ GPa), which is in accord with our prediction that $[B_{12}(N-N)]_{0.33}[B_{12}(NBN)]_{0.67}$ is also thermodynamically stable at low pressures; see Fig. 7.

Furthermore, upon cooling the mixtures between liquid boron and h-BN from $T > 2300$ K at $p \approx 5$ GPa and at different fixed contents of N, Solozhenko *et al.* [33] found that at 3.8 at. % N, equivalent to the $B_{50}N_2$ composition, the quenched sample consisted of a β-boron and α-tetragonal-boron-like phase, given by t-$B_{50}N_{2-x}B_x$, and the formation of αR-boron-like boron subnitride is absent at this composition. This is also in accord with our predictions that, at the global composition of $B_{50}N_2$, only t-$B_{50}N_2$ is found to be thermodynamically stable up to at least 10 GPa, depending on the temperature, before it decomposes into pure boron and c-BN.

We also find that the simulated x-ray powder-diffraction pattern of $[B_{12}(N-N)]_{0.33}[B_{12}(NBN)]_{0.67}$, obtained from the RIETAN-FP package [79] as implemented in VESTA [80], is in good agreement with the experimental powder-diffraction data of $B_6N_{0.92}$ [30] and $B_{13}N_2$ [32], taken from The International Centre for Diffraction Data (ICDD) cards: 00-050-1504 and 00-060-0209, respectively, as shown in Fig. 8. We thus conclude that $B_{36}N_6$ is the stable composition of αR-boron-like boron subnitride, whose atomic configuration is given by the mixture between B_{12}(N-N) and B_{12}(NBN) with the ratio of 1:2, denoted by $[B_{12}(N-N)]_{0.33}[B_{12}(NBN)]_{0.67}$, while the B_6N and $B_{13}N_2$ compositions, solely represented by B_{12}(N-N) and B_{12}(NBN), respectively, are not found to be thermodynamically stable at any pressure and temperature.

As a consequence, we further suggest that the experimentally synthesized αR-boron-like boron subnitrides, denoted by $B_6N_{0.92}$ [30] and $B_{13}N_2$ [31–33] compositions in the literature, should also be represented by the mixtures between B_{12}(N-N) and B_{12}(NBN) with the global compositions of about $B_{38}N_6$, where the concentrations of B_{12}(N-N) and B_{12}(NBN) possibly deviate from those of $B_{38}N_6$ in the dilute limit, as indicated by the small variation of lattice parameters between $B_6N_{0.92}$ [30] and $B_{13}N_2$ [31–33], measured from the experiments, and $[B_{12}(N-N)]_{0.33}[B_{12}(NBN)]_{0.67}$, calculated in this work; see Table II. This is also in accord with the suggestion, given by Solozhenko *et al.* [32], that rather than a solid solution like boron carbide, αR-boron-like boron subnitride is a line compound.

IV. CONCLUSION

We examine using first-principles calculations the thermodynamic stability as a function of pressure and temperature of three different αR-boron-like boron subnitrides, proposed in the literature; those are B_6N represented by B_{12}(N-N), $B_{13}N_2$ represented by B_{12}(NBN), and $B_{38}N_6$ represented by $[B_{12}(N-N)]_{0.33}[B_{12}(NBN)]_{0.67}$, with respect to their relevant competing phases. We find that, among the three considered boron subnitrides, only $B_{38}N_6$, $[B_{12}(N-N)]_{0.33}[B_{12}(NBN)]_{0.67}$, is thermodynamically stable from 0 GPa up to ~7.5 GPa, depending on the temperature. Beyond this pressure, $[B_{12}(N-N)]_{0.33}[B_{12}(NBN)]_{0.67}$ becomes unstable and decomposes into cubic boron nitride and α-tetragonal-boron-like boron subnitride, t-$B_{50}N_2$. This is in a good agreement in terms of conditions for experimental

syntheses of αR-boron-like boron subnitrides, reported in the literature. By inspecting its elastic constants, phonon and electronic density of states, $[B_{12}(N-N)]_{0.33}[B_{12}(NBN)]_{0.67}$ is found mechanically and dynamically stable, and is an electrical semiconductor with the GGA-estimated electronic band gap of 0.7 eV.

By comparing the calculated lattice parameters as well as the simulated x-ray powder-diffraction pattern of $[B_{12}(N-N)]_{0.33}[B_{12}(NBN)]_{0.67}$ to those of the experimentally synthesized αR-boron-like boron subnitrides, we suggest that, instead of being represented solely by B_{12}(N-N) or B_{12}(NBN) as often claimed previously, the experimentally synthesized αR-boron-like boron subnitrides should be described by $B_{38}N_6$, where the mixtures of the structural units are represented by $[B_{12}(N-N)]_{0.33}[B_{12}(NBN)]_{0.67}$. We thus conclude that $B_{38}N_6$, represented by $[B_{12}(N-N)]_{0.33}[B_{12}(NBN)]_{0.67}$, is the stable composition of αR-boron-like boron subnitride.

ACKNOWLEDGMENTS

Financial support by the Swedish Research Council (VR) through Young Researcher Grant No. 621-2011- 4417 and International Career Grant No. 330-2014-6336 and Marie Sklodowska Curie Actions, Cofund, Project INCA 600398, is gratefully acknowledged by B.A. The support from CeNano at Linköping University is acknowledged by A.E. and B.A. S.I.S. acknowledges Swedish Research Council (VR) Project No. 2014-4750. B.A. and S.I.S acknowledge support from the Swedish Government Strategic Research Area in Materials Science on Functional Materials at Linköping University (Faculty Grant SFO-Mat-LiU No. 2009 00971). The simulations were carried out using supercomputer resources provided by the Swedish National Infrastructure for Computing (SNIC) performed at the National Supercomputer Centre (NSC) and the Center for High Performance Computing (PDC).

[1] Z. Zhang, E. S. Penev, and B. I. Yakobson, Two-dimensional materials: Polyphony in B flat, Nat. Chem. **8**, 525 (2016).

[2] B. Feng, J. Zhang, Q. Zhong, W. Li, S. Li, H. Li, P. Cheng, S. Meng, L. Chen, and K. Wu, Experimental realization of two-dimensional boron, Nat. Chem. **8**, 563 (2016).

[3] A. J. Mannix, X.-F. Zhou, B. Kiraly, J. D. Wood, D. Alducin, B. D. Myers, X. Liu, B. L. Fisher, U. Santiago, J. R. Guest, M. J. Yacaman, A. Ponce, A. R. Oganov, M. C. Hersam, and N. P. Guisinger, Synthesis of borophenes: Anisotropic, two-dimensional boron polymorphs, Science **350**, 1513 (2015).

[4] J. Tian, Z. Xu, C. Shen, F. Liu, N. Xu, and H.-J. Gao, One-dimensional boron nanostructures: Prediction, synthesis, characterizations, and applications, Nanoscale **2**, 1375 (2010).

[5] M. Liu, V. I. Artyukhov, and B. I. Yakobson, Mechanochemistry of one-dimensional boron: Structural and electronic transitions, J. Am. Chem. Soc. **139**, 2111 (2017).

[6] F. Thevénot, Boron carbide - A comprehensive review, J. Eur. Ceram. Soc. **6**, 205 (1990).

[7] V. Domnich, S. Reynaud, R. A. Haber, and M. Chhowalla, Boron carbide: Structure, properties, and stability under stress, J. Am. Ceram. Soc. **94**, 3605 (2011).

[8] D. Emin, Unusual properties of icosahedral boron-rich solids, J. Solid State Chem. **179**, 2791 (2006).

[9] D. Emin, Icosahedral boron-rich solids, Phys. Today **40**(1), 55 (1987).

[10] M. Carrard, D. Emin, and L. Zuppiroli, Defect clustering and self-healing of electron-irradiated boron-rich solids, Phys. Rev. B **51**, 11270 (1995).

[11] A. Hushur, M. H. Manghnani, H. Werheit, P. Dera, and Q. Williams, High-pressure phase transition makes $B_{4.3}C$ boron carbide a wide-gap semiconductor, J. Phys.: Condens. Matter **28**, 045403 (2016).

[12] S. V. Ovsyannikov, A. Polian, P. Munsch, J.-C. Chervin, G. Le Marchand, and T. L. Aselage, Raman spectroscopy of $B_{12}As_2$ and $B_{12}P_2$ up to 120 GPa: Evidence for structural distortion, Phys. Rev. B **81**, 140103(R) (2010).

[13] C. D. Frye, J. H. Edgar, I. Ohkubo, and T. Mori, Seebeck coefficient and electrical resistivity of single crystal $B_{12}As_2$ at high temperatures, J. Phys. Soc. Jpn. **82**, 095001 (2013).

[14] M. Herrmann, I. Sigalas, M. Thiele, M. M. Müller, H. J. Kleebe, and A. Michaelis, Boron suboxide ultrahard materials, Int. J. Refract. Hard Met. **39**, 53 (2013).

[15] T. L. Aselage, D. Emin, C. Wood, I. Mackinnon, and I. Howard, Anomalous seebeck coefficient in boron carbides, MRS Proc. **97**, 27 (1987).

[16] S. Adenwalla, P. Welsch, A. Harken, J. I. Brand, A. Sezer, and B. W. Robertson, Boron carbide/*n*-silicon carbide heterojunction diodes, Appl. Phys. Lett. **79**, 4357 (2001).

[17] H. Werheit, Boron-rich solids: a chance for high-efficiency high-temperature thermoelectric energy conversion, Mater. Sci. Eng. B **29**, 228 (1995).

[18] D. Emin and T. L. Aselage, A proposed boron-carbide-based solid-state neutron detector, J. Appl. Phys. **97**, 013529 (2005).

[19] C. Höglund, J. Birch, K. Andersen, T. Bigault, J.-C. Buffet, J. Correa, P. van Esch, B. Guerard, R. Hall-Wilton, J. Jensen, A. Khaplanov, F. Piscitelli, C. Vettier, W. Vollenberg, and L. Hultman, B_4C thin films for neutron detection, J. Appl. Phys. **111**, 104908 (2012).

[20] Y. Gong, M. Tapajna, S. Bakalova, Y. Zhang, J. H. Edgar, Y. Zhang, M. Dudley, M. Hopkins, and M. Kuball, Demonstration of boron arsenide heterojunctions: A radiation hard wide band gap semiconductor device, Appl. Phys. Lett. **96**, 223506 (2010).

[21] C. E. Whiteley, Y. Zhang, Y. Gong, S. Bakalova, A. Mayo, J. H. Edgar, and M. Kuball, Semiconducting icosahedral boron arsenide crystal growth for neutron detection, J. Cryst. Growth **318**, 553 (2011).

[22] O. O. Kurakevych and V. L. Solozhenko, Experimental study and critical review of structural, thermodynamic and mechanical properties of superhard refractory boron suboxide B_6O, J. Superhard Mater. **33**, 421 (2011).

[23] G. A. Slack and K. E. Morgan, Some crystallography, chemistry, physics, and thermodynamics of $B_{12}O_2$, $B_{12}P_2$, $B_{12}As_2$, and related alpha-boron type crystals, J. Phys. Chem. Solids **75**, 1054 (2014).

[24] G. A. Slack and K. E. Morgan, Crystallography, semiconductivity, thermoelectricity, and other properties of boron and its compounds, especially B_6O, Solid State Sci. **47**, 43 (2015).

[25] J. Wu, H. Zhu, D. Hou, C. Ji, C. E. Whiteley, J. H. Edgar, and Y. Ma, High pressure X-ray diffraction study on icosahedral boron arsenide ($B_{12}As_2$), J. Phys. Chem. Solids **72**, 144 (2011).

[26] C. E. Whiteley, M. J. Kirkham, and J. H. Edgar, The coefficients of thermal expansion of boron arsenide ($B_{12}As_2$) between 25 °C and 850 °C, J. Phys. Chem. Solids **74**, 673 (2013).

[27] S. Bakalova, Y. Gong, C. Cobet, N. Esser, Y. Zhang, J. H. Edgar, Y. Zhang, M. Dudley, and M. Kuball, Energy band structure and optical response function of icosahedral $B_{12}As_2$: A spectroscopic ellipsometry and first-principles calculational study, Phys. Rev. B **81**, 075114 (2010).

[28] J. B. Condon, C. E. Holcombe, D. H. Johnson, and L. M. Steckel, The kinetics of the boron plus nitrogen reaction, Inorg. Chem. **15**, 2173 (1976).

[29] H. Saitoh, K. Yoshida, and W. A. Yarbrough, Crystal structure of new composition boron-rich boron nitride using Raman spectroscopy, J. Mater. Res. **8**, 8 (1993).

[30] H. Hubert, L. A. J. Garvie, P. R. Buseck, W. T. Petuskey, and P. F. McMillan, High-pressure, high-temperature syntheses in the B–C–N–O system, J. Solid State Chem. **133**, 356 (1997).

[31] V. L. Solozhenko and O. O. Kurakevych, New boron subnitride $B_{13}N_2$: HP-HT synthesis, structure and equation of state, J. Phys.: Conf. Ser. **121**, 062001 (2008).

[32] V. L. Solozhenko and O. O. Kurakevych, Chemical interaction in the B-BN system at high pressures and temperatures. Synthesis of novel boron subnitrides, J. Solid State Chem. **182**, 1359 (2009).

[33] V. L. Solozhenko, O. O. Kurakevych, V. Z. Turkevich, and D. V. Turkevich, Phase diagram of the B-BN system at 5 GPa, J. Phys. Chem. B **114**, 5819 (2010).

[34] H. Zhang, S. Yao, and M. Widom, Predicted phase diagram of boron-carbon-nitrogen, Phys. Rev. B **93**, 144107 (2016).

[35] V. L. Solozhenko, Y. L. Godec, and O. O. Kurakevych, Solid-state synthesis of boron subnitride, B_6N: myth or reality? C. R. Chim. **9**, 1472 (2006).

[36] D. M. Bylander and L. Kleinman, Structure of $B_{13}C_2$, Phys. Rev. B **43**, 1487 (1991).

[37] J. E. Saal, S. Shang, and Z. K. Liu, The structural evolution of boron carbide via *an initio* calculations, Appl. Phys. Lett. **91**, 231915 (2007).

[38] N. Vast, J. Sjakste, and E. Betranhandy, Boron carbides from first principles, J. Phys.: Conf. Ser. **176**, 012002 (2009).

[39] A. Ektarawong, S. I. Simak, L. Hultman, J. Birch, and B. Alling, Configurational order-disorder induced metal-nonmetal transition in $B_{13}C_2$ studied with first-principles superatom-special quasirandom structure method, Phys. Rev. B **92**, 014202 (2015).

[40] L. Cao, H. T. Zhang, M. Feng, Z. Zhan, W. Wang, and X. Zhang, Heterostructured B_6N_x/BN nanocable and nanofeather nanojunctions, Cryst. Growth Des. **8**, 4350 (2008).

[41] P. E. Blöchl, Projector augmented-wave method, Phys. Rev. B **50**, 17953 (1994).

[42] G. Kresse and J. Furthmüller, Efficiency of ab-initio total energy calculations for metals and semiconductors using a plane-wave basis set, Comput. Mater. Sci. **6**, 15 (1996).

[43] G. Kresse and J. Furthmüller, Efficient iterative schemes for *abinitio* total-energy calculations using a plane-wave basis set, Phys. Rev. B **54**, 11169 (1996).

[44] J. Perdew, K. Burke, and M. Ernzerhof, Generalized Gradient Approximation Made Simple, Phys. Rev. Lett. **77**, 3865 (1996).

[45] H. J. Monkhorst and J. D. Pack, Special points for Brillouin-zone integrations, Phys. Rev. B **13**, 5188 (1976).

[46] P. E. Blöchl, O. Jepsen, and O. K. Andersen, Improved tetrahedron method for brillouin-zone integrations, Phys. Rev. B **49**, 16223 (1994).

[47] A. Ektarawong, S. I. Simak, L. Hultman, J. Birch, and B. Alling, First-principles study of configurational disorder in B_4C using a superatom-special quasirandom structure method, Phys. Rev. B **90**, 024204 (2014).

[48] A. Ektarawong, S. I. Simak, L. Hultman, J. Birch, F. Tasnádi, F. Wang, and B. Alling, Effects of configurational disorder on the elastic properties of icosahedral boron-rich alloys based on B_6O, $B_{13}C_2$, and B_4C, and their mixing thermodynamics, J. Chem. Phys. **144**, 134503 (2016).

[49] A. Togo and I. Tanaka, First principles phonon calculations in material science, Scr. Mater. **108**, 1 (2015).

[50] A. Togo, F. Oba, and I. Tanaka, First-principles calculations of the ferroelastic transition between rutile-type and $CaCl_2$-type SiO_2 at high pressures, Phys. Rev. B **78**, 134106 (2008).

[51] K. Parlinski, Z. Q. Li, and Y. Kawazoe, First-Principles Determination of the Soft Mode in Cubic ZrO_2, Phys. Rev. Lett. **78**, 4063 (1997).

[52] F. D. Murnaghan, On the theory of the tension of an elastic cylinder, Proc. Natl. Acad. Sci. USA **30**, 382 (1944).

[53] F. Birch, Finite elastic strain of cubic crystals, Phys. Rev. **71**, 809 (1947).

[54] R. Golesorkhtabar, P. Pavone, J. Spitaler, P. Puschnig, and C. Draxl, ElaStic: A tool for calculating second-order elastic constants from first principles, Comput. Phys. Commun. **184**, 1861 (2013).

[55] F. Tasnádi, M. Odén, and I. A. Abrikosov, *Ab initio* elastic tensor of cubic $Ti_{0.5}Al_{0.5}N$ alloys: Dependence of elastic constants on size and shape of the supercell model and their convergence, Phys. Rev. B **85**, 144112 (2012).

[56] J. F. Nye, *Physical Properties of Crystals: Their Representation by Tensors and Matrices* (Oxford University Press, New York, 1985).

[57] L. Vitos, *Computational Quantum Mechanics for Materials Engineers: The EMTO Method and Applications (Engineering Materials and Processes)* (Springer, Berlin, 2010).

[58] M. Moakher and A. N. Norris, The closest elastic tensor of arbitrary symmetry to an elasticity tensor of lower symmetry, J. Elast. **85**, 215 (2006).

[59] F. Mouhat and F.-X. Coudert, Necessary and sufficient elastic stability conditions in various crystal systems, Phys. Rev. B **90**, 224104 (2014).

[60] G. Simmons and H. Wang, *Single Crystal Elastic Constants and Calculated Aggregate Properties: A Handbook* (MIT Press, Cambridge, MA, 1971).

[61] H. Gou, J. Zhang, and F Gao, First-principles calculations of boron-rich compounds of $B_{13}N_2$ and $B_{12}C_2X$ (X = Si, Ge), J. Phys.: Condens. Matter **20**, 505211 (2008).

[62] A. R. Oganov, J. Chen, C. Gatti, Y. Ma, Y. Ma, C. W. Glass, Z. Liu, T. Yu, O. O. Kurakevych, and V. L. Solozhenko, Ionic high-pressure form of elemental boron, Nature (London) **457**, 863 (2009).

[63] E. Yu. Zarechnaya, L. Dubrovinsky, N. Dubrovinskaia, Y. Filinchuk, D. Chernyshov, V. Dmitriev, N. Miyajima, A. El Goresy, H. F. Braun, S. Van Smaalen, I. Kantor, A. Kantor, V. Prakapenka, M. Hanfland, A. S. Mikhaylushkin, I. A. Abrikosov,

and S. I. Simak, Superhard Semiconducting Optically Transparent High Pressure Phase of Boron, Phys. Rev. Lett. **102**, 185501 (2009).

[64] S. Bohr, R. Haubner, and B. Lux, Comparative aspects of c-BN and diamond CVD, Diamond Relat. Mater. **4**, 714 (1995).

[65] V. L. Solozhenko, V. Z. Turkevich, and W. B. Holzapfel, Refined Phase Diagram of Boron Nitride, J. Phys. Chem. B **103**, 2903 (1999).

[66] G. Kern, G. Kresse, and J. Hafner, *Ab initio* calculation of the lattice dynamics and phase diagram of boron nitride, Phys. Rev. B **59**, 8551 (1999).

[67] N. Ohba, K. Miwa, N. Nagasako, and A. Fukumoto, First-principles study on structural, dielectric, and dynamical properties for three BN polytypes, Phys. Rev. B **63**, 115207 (2001).

[68] W. J. Yu, W. M. Lau, S. P. Chan, Z. F. Liu, and Q. Q. Zheng, *AB initio* study of phase transformations in boron nitride, Phys. Rev. B **67**, 014108 (2003).

[69] M. Halo, C. Pisani, L. Maschio, S. Casassa, M. Schütz, and D. Usvyat, Electron correlation decides the stability of cubic versus hexagonal boron nitride, Phys. Rev. B **83**, 035117 (2011).

[70] K. Ploog, H. Schmidt, E. Amberger, G. Will, and K. H. Kossobutzki, $B_{48}B_2C_2$ UND $B_{48}B_2N_2$, Zwei nichtmetallboride mit der struktur des Sog. I tetragonalen bors, J. Less-Common Met. **29**, 161 (1972).

[71] I. Morrison, D. M. Bylander, and L. Kleinman, Computational study of tetragonal $B_{50}N_2$, Phys. Rev. B **45**, 10872 (1992).

[72] N. Uemura, K. Shirai, H. Eckert, and J. Kunstmann, Structure, nonstoichiometry, and geometrical frustration of α-tetragonal boron, Phys. Rev. B **93**, 104101 (2016).

[73] X. Guo, J. He, Z. Liu, Y. Tian, J. Sun, and H. T. Wang, Bond ionicities and hardness of $B_{13}C_2$-like structured B_yX crystals (X=C, N, O, P, As), Phys. Rev. B **73**, 104115 (2006).

[74] H. C. Longuet-Higgins and M. de V. Roberts, The electronic structure of an icosahedron of boron atoms, Proc. R. Soc. London, Ser. A **230**, 110 (1955).

[75] S. F. Pugh, XCII. Relations between the elastic moduli and the plastic properties of polycrystalline pure metals, Lond. Edinb. Dubl. Phil. Mag. 7 **45**, 823 (1954).

[76] S. Yao, W. P. Huhn, and M. Widom, Phase transitions of boron carbide: Pair interaction model of high carbon limit, Solid State Sci. **47**, 21 (2015).

[77] J. W. D. Connolly and A. R. Williams, Density-functional theory applied to phase transformations in transition-metal alloys, Phys. Rev. B **27**, 5169(R) (1983).

[78] N. Metropolis, A. W. Rosenbluth, M. N. Rosenbluth, A. H. Teller, and Edward Teller, Equation of state calculations by fast computing machines, J. Chem. Phys. **21**, 1087 (1953).

[79] F. Izumi and K. Momma, Three-dimensional visualization in powder diffraction, Solid State Phenom. **130**, 15 (2007).

[80] K. Momma and F. Izumi, *VESTA3* for three-dimensional visualization of crystal, volumetric and morphology data, J. Appl. Crystallogr. **44**, 1272 (2011).